Journal of Materials Chemistry B

PAPER

View Article Online
View Journal | View Issue

Cite this: J. Mater. Chem. B, 2019, 7, 7042

High-activity Mo, S co-doped carbon quantum dot nanozyme-based cascade colorimetric biosensor for sensitive detection of cholesterol†

Lianjing Zhao,[a] Zepei Wu,[a] Guannan Liu,[a] Huiying Lu,[a] Yuan Gao,*[a] Fangmeng Liu,[a] Chenguang Wang,[a] Jiuwei Cui*[b] and Geyu Lu*[a]

Received 14th August 2019,
Accepted 8th October 2019

DOI: 10.1039/c9tb01731c

rsc.li/materials-b

Nanozymes have drawn considerable attention because of their lower cost, higher stability and convenient preparation compared to protein enzymes. In the present work, Mo, S co-doped carbon quantum dots (Mo-CQDs) as a peroxidase mimic were used to fabricate a cascade colorimetric biosensor to detect cholesterol. The Mo-CQDs possess a robust peroxidase-like activity, and they can easily catalyze 3,3,5,5-tetramethylbenzidine (TMB) to produce an oxidized TMB in the presence of H_2O_2. The Mo, S doping in the carbon quantum dots (CQDs) notably boosts the yield of CQDs and may facilitate the electron transfer between TMB and H_2O_2, which further enhances the catalytic activity of CQDs. The colorimetric biosensor based on Mo-CQDs and cholesterol oxidase exhibited excellent selectivity and high sensitivity for cholesterol in the range of 0.01–1.0 mM along with a detection limit as low as 7 μM. The total cholesterol concentration in the serum sample was measured with satisfactory results and read out by the naked eye, indicating the potential application in clinical diagnosis and portable test kits.

1 Introduction

Cholesterol, extensively existing in human blood, participates in the formation of cell membranes and is a precursor for the synthesis of some important biomolecules such as bile acids, vitamin D and steroid hormones. Although cholesterol is of crucial importance in organisms, it is essential to maintain it in an optimum range from 2.9 to 6.0 mM in serum of healthy adults.[1] Research indicated that abnormal cholesterol levels over a long term are associated with various diseases, such as cardiovascular and cerebrovascular diseases, lipid metabolism disorder and anemia.[2–5] Thus, there is clinical significance in precisely detecting cholesterol for early diagnosis of diseases. Various approaches have been developed to detect cholesterol, such as colorimetry, fluorescence, chromatography, electrochemical analysis and chemiluminescence.[6–8] Among them, the colorimetric method based on horseradish peroxidase (HRP) is widely applied in clinical diagnosis because of its safety, specificity, simplification and ease of automatic detection. Furthermore, the results of the colorimetric method can be visually and simply read out by the naked eye.[9] However, HRP suffers from some serious drawbacks, such as easy denaturation, high-cost and complex preparation and purification processes, which restrict its practical application.

Recently, nanozymes (nanomaterials with enzyme-like activity), as a candidate of an ideal and important tool of colorimetric methods, have attracted tremendous attention due to their lower cost, higher stability and more convenient preparation than protein enzymes.[10–14] Inorganic nanomaterials with peroxidase-like activity, such as transition metal oxides (*e.g.* ferromagnetic nanoparticles),[15–17] transition metal sulfides (*e.g.* AuNP@MoS_2QD, nanohybrids of gold nanoparticles and MoS_2 nanoribbons[18,19]), carbon-based nanomaterials (*e.g.* graphene dots,[20] graphene,[21,22] and carbon nanotubes[23]) and other nonmetallic nanomaterials (*e.g.* silicon dots,[24] and CeO_2[25]), were explored and used to construct colorimetric sensors. To date, a few two-dimensional nanozymes (MoS_2 nanosheets and CuS nanocomposites) and Fe_3O_4 nanoparticles have been explored to fabricate cholesterol biosensors.[26–28] Although these nanomaterials have exhibited promising peroxidase-mimic activity, they have prominent disadvantages including harsh synthetic conditions, high-cost or low water solubility.

Taking advantage of their good water solubility and stability, biocompatibility, environmentally benign nature and large specific surface area, zero-dimension carbon nanomaterials are attractive as peroxidase mimics, and they can also provide

[a] State Key Laboratory on Integrated Optoelectronics, College of Electronic Science and Engineering, Jilin University, 2699 Qianjin Street, Changchun 130012, China. E-mail: gaoyuan@jlu.edu.cn, lugy@jlu.edu.cn; Tel: +86 431 85168384, +86 431 85167808

[b] Cancer Center, The First Hospital of Jilin University, Changchun 130021, China. E-mail: cuijw@jlu.edu.cn; Tel: +86 431 88786134

† Electronic supplementary information (ESI) available. See DOI: 10.1039/c9tb01731c

more active sites.[29–31] As one kind of carbon nanomaterial with zero-dimension, graphene quantum dots (GQDs) derived from graphene-based materials have exerted peroxidase-like activity.[32] However, the synthesis process of these GQDs needs severe synthetic conditions and the peroxidase-like activity of these GQDs still requires further improvement.[33,34] To overcome these limitations, heteroatom doping may be an effective strategy to develop carbon quantum dot (CQD) based nanozymes with the properties of low-cost, easy manipulation and high efficient catalytic activity. Nonmetal element doping (nitrogen and sulfur) in CQDs has been reported,[33,35,36] but the research of metal doping in CQDs especially CQDs with peroxidase-like activity is still in its infancy. To date, only a few references reported that platinum and copper doped CQDs exhibited high peroxidase-like activity.[37,38] Taking the safety, low-cost and high peroxidase-like activity of MoS_2 quantum dots and nanosheets into consideration,[39–41] molybdenum and sulfur were selected to be co-doped in CQDs. The CQDs co-doped with molybdenum and sulfur were expected to act as nanozymes with high peroxidase-like activity, good dispersion and low cost.

In the present work, we prepared Mo, S co-doped carbon quantum dots (Mo-CQDs) with high peroxidase mimetic catalytic activity and excellent dispersion by the one step solvothermal treatment of ethanol with the assistance of MoS_2 powder. Ethanol was simultaneously employed as a carbon source and solvent. The approach was economical as it used only two reagents, a large amount of ethanol and a small amount of MoS_2 powder. In addition, a simple and facile manufacturing process and high catalytic activity also made the Mo-CQDs ideal candidates of nanozymes. The Mo, S doping could not only notably enhance the yield of CQDs but also facilitated the increase of catalytic activity of CQDs. The Mo-CQDs with high peroxidase mimetic catalytic activity combined with cholesterol oxidase cascade reaction were utilized to construct biosensors for the sensitive detection of cholesterol. Furthermore, the results of the determination could be visualized by the naked eye without the assistance of any specialized instruments, suitable for the preparation of a portable cholesterol test kit. The total cholesterol in different human serum samples was exactly measured. Thus, the fabricated biosensor exhibits potential utility in visual platforms for effective cholesterol detection and clinical diagnosis.

2 Materials and methods

2.1 Materials and apparatus

L-Cysteine, molybdenum disulfide and glutathione were obtained from Aladdin Industrial Co., Ltd (Shanghai, China). Cholesterol, 3,3′,5,5′-tetramethylbenzidine (TMB), cholesterol oxidase and cholesterol esterase were provided by Sigma Aldrich (USA). Urea and L-ascorbic acid (vitamin C) were obtained from Dingguo Biotech Co., Ltd (Beijing, China). Hydrogen peroxide (H_2O_2), anhydrous ethanol, uric acid, glucose, monobasic potassium phosphate (KH_2PO_4) and dipotassium phosphate (K_2HPO_4) were purchased from Sinopharm Chemical Reagent Co., Ltd (Shanghai, China). Volunteers' serum was supplied by the First Hospital of Jilin University. This study was approved by the Research Ethics Board of the First Hospital of Jilin University. All solutions were prepared in deionized distilled water. All chemical reagents were of analytical grade without further purification.

The UV-vis spectra were determined on a UV-2550 UV-vis spectrophotometer (Shimadzu, Japan) and fluorescence spectral measurements were performed on an RF-5301PC fluorophotometer (Shimadzu, Japan). Fourier Transform infrared (FTIR) spectral measurements were carried out on a Nicolet iS10 FTIR spectrometer with an attenuated total reflectance (ATR) accessory (Thermo scientific, America), which was employed to investigate the surface groups of Mo-CQDs. A Thermo ESCALAB 250 spectrometer (Thermo scientific, America) was used to record X-ray photoelectron spectroscopy (XPS) spectra. Transmission electron microscopy (TEM) and high solution transmission electron microscopy (HRTEM) images of Mo-CQDs were obtained by using a JEOL TEM-3010 instrument. X-ray diffraction (XRD) patterns of the Mo-CQDs were recorded by using a Rigaku wide-angle X-ray diffractometer. The measurement of fluorescent quantum yield of the Mo-CDs was performed by using an Edinburgh FLS920 phosphorimeter (Edinburgh Instruments, U.K.).

2.2 Preparation of Mo-CQDs

The Mo-CQDs were synthesized by the one step solvothermal treatment of ethanol in the presence of MoS_2. Briefly, a mixture of 80 mL of ethanol and 40 mg of MoS_2 power was ultrasonicated for 8 h, then the mixture was transferred into a 50 mL Teflon-lined stainless steel autoclave for reaction for 12 h at 200 °C. Then, the large size MoS_2 was removed by filtering with a 0.22 μm microporous membrane and the reaction solution was further dialyzed by a dialysis bag (molecular weight cut off: 3000 Da) for two days. The solid product was obtained by vacuum freeze drying of the outer dialysate.

2.3 Procedures for H_2O_2 detection

For H_2O_2 detection, 20 μL of 15 mM TMB, 10 μL of 100 μg mL^{-1} Mo-CQDs and 260 μL of 0.2 M sodium acetate buffer (pH 4.0) were mixed, and then different concentrations of H_2O_2 (10 μL) were added. After 30 min of incubation at room temperature, the UV-vis absorption spectrum was determined immediately. Each experiment was repeated three times.

2.4 Optimization procedure of cholesterol determination

Cholesterol detection was carried out as follows: first, 5 μL of 100 UN mL^{-1} cholesterol oxidase, 10 μL of different concentrations of CHO and 35 μL of 0.5 mM phosphate buffer (pH 7.0) were mixed and incubated for 30 min at 37 °C, and then 10 μL of 100 μg mL^{-1} Mo-CQDs, 20 μL of 15 mM TMB and 260 μL of 0.2 M sodium acetate buffer (pH 4.0) were added into the above mixture. After 30 min of incubation at 37 °C for 30 min, the UV-vis absorption spectrum was determined immediately. To examine the specificity for cholesterol detection, uric acid, urea, glucose, ascorbic acid and cysteine were added into the reaction solution instead of cholesterol followed by performing the same cholesterol detection process, respectively. Each experiment was repeated three times.

2.5 Detection of total cholesterol in human serum samples

Detection of total cholesterol in human serum was performed as follows: first, 5.0 μL of 100 UN mL^{-1} cholesterol oxidase, 5.0 μL of 100 UN mL^{-1} cholesterol esterase, 2.0 μL volunteers' serum and 38 μL of 0.5 mM phosphate buffer (pH 7.0) were mixed and incubated at 37 °C for 30 min. Then, 10 μL of Mo-CQDs (100 μg mL^{-1}), 20 μL of TMB (15 mM) and 260 μL of sodium acetate buffer (0.2 M, pH 4.0) were added. After 30 min of incubation at 37 °C for 30 min, the UV-vis absorption spectrum was determined immediately. Each experiment was repeated three times.

3 Results and discussion

3.1 Preparation and characterization of Mo-CQDs

Mo, S co-doped CQDs (Mo-CQDs) were prepared by a simple solvothermal synthesis of MoS_2 powder in ethanol, followed by dialysis purification. Ethanol simultaneously played the dual-role of carbon source and solvent in the synthesis. The TEM images showed that synthesized Mo-CQDs were spherical and had good dispersion (Fig. 1a). The inset of Fig. 1a reveals that the lateral diameter of obtained Mo-CQDs ranged from 3 nm to 5.5 nm with an average size of about 4.1 nm. In addition, the HRTEM image revealed high crystallinity of Mo-CQDs and the lattice spacing of the Mo-CQDs was 0.21 nm (Fig. 1b), which was assigned to the (100) lattice distance of the graphitic carbon.[42,43] Interestingly, the Mo-CQDs exhibited a long-term stability in water without obvious precipitation at 4 °C for several months of storage, which facilitated their applications in bio-sensing and clinical diagnosis.

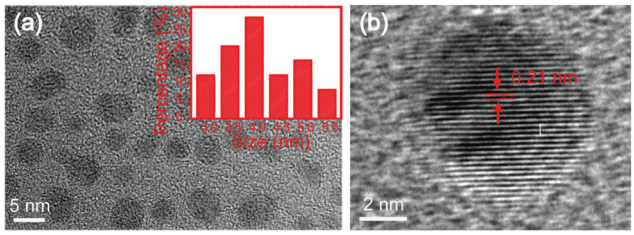

Fig. 1 (a) TEM image of the Mo-CQDs. (b) HRTEM image of the Mo-CQDs. The inset of (a) is size distribution of the Mo-CQDs.

The XPS and FTIR spectra were employed to investigate the chemical composition and surface groups of Mo-CQDs. In the XPS spectra (Fig. 2a), the peaks at 284, 530.6, 497.5, 232.3, and 168.7 eV were attributed to C 1s, O 1s, Mo 3s, Mo 3d, and S 2p, respectively.[44] XPS analysis revealed that the atomic% of Mo, S, C and O was 0.55%, 4.52%, 36.6% and 56.8%, respectively. These results indicated that the sample mainly consisted of carbon and oxygen, and contained small amounts of molybdenum and sulfur. Most of the bulk MoS_2 was removed during filtration and dialysis in the process of synthesis. In the high resolution XPS spectra of C 1s (Fig. 2b), the C 1s core region of the spectrum could be resolved into three peaks at 284.6, 285.6, 288, 289.3 and 292.8 eV, assigned to graphitic (C–C/C═C) sp^2 carbon, C–S/C–O bonds, carbonyl (C═O) carbons and carboxyl (–COOH) carbon, respectively.[45–48] In the S 2p spectra (Fig. 2c), the two distinct peaks centered at high energy (168.6 eV and 169.7 eV) were consistent with the reported –C–$S(O)_2$–C– sulphone bridges.[49,50] Another peak at 163.8 eV could be attributed to –C–S–C– sulphide bridges.[51,52] The binding energy of the S atoms in the sulphide

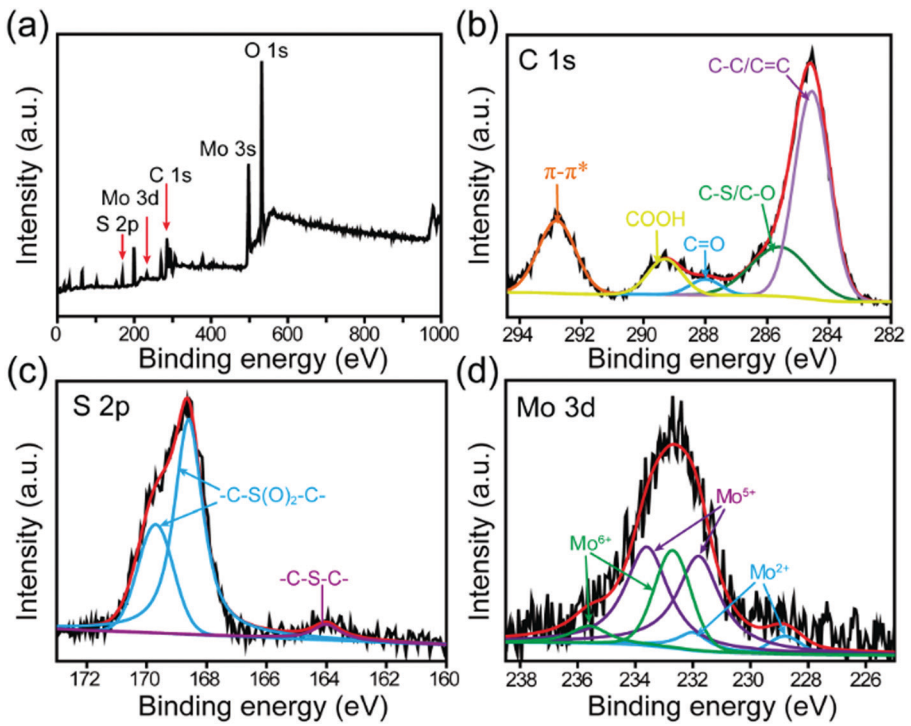

Fig. 2 (a) XPS spectra of Mo-CQDs. (b, c and d) High resolution XPS spectra of C 1s, S 2p and Mo 3d.

bridges and sulphone bridges was higher than that of the original MoS_2 (Fig. S1a in the ESI†), suggesting that most of the S atoms were oxidized and existed in C–S covalent bonds. The high resolution Mo 3d XPS spectra (Fig. 2d) could be resolved into six peaks, wherein the peaks at 235.6 and 232.8 eV are ascribed to Mo^{6+}, the peaks at 233.6 and 231.8 eV are assigned to Mo^{5+}, and the peaks at 232 and 228.8 eV were attributed to Mo^{2+}. The high resolution Mo 3d XPS spectra in the pristine bulk MoS_2 could be resolved into three peaks, wherein the peaks at 232.8 and 229.7 eV were attributed to Mo^{4+} (Fig. S1b, ESI†). The binding energy of Mo^{2+} was lower than that of Mo 3d in the pristine bulk MoS_2, which was in good agreement with Mo peaks in Mo_2C.[53] The analysis of Mo 3d at the higher binding energy demonstrated that most of the Mo atoms were oxidized and existed in the form of Mo–O covalent bonds. As shown in Fig. 3a, the FTIR spectra of Mo-CQDs displayed the characteristic absorptions of C=O stretching vibration at 1640 cm^{-1}, C–O stretching vibration at 1394 cm^{-1},[54] C–O–C stretching vibration at 1112 cm^{-1}, C–H stretching vibration at 2978 cm^{-1},[55] and C–S stretching vibrations at 922 cm^{-1} and 780 cm^{-1}.[50] Mo-CQDs were functionalized with polar functional groups such as carbonyl, carboxylic acid and hydroxyl. These functional groups of Mo-CQDs guaranteed their excellent solubility. The XPS and FTIR results demonstrated that most of the Mo atoms and S atoms in Mo-CQDs existed in the Mo–O, Mo–C and C–S covalent bonds and a small quantity of Mo and S was doped into Mo-CQDs. The crystal structure and composition of Mo-CQDs were further characterized by XRD. As presented in Fig. 3b, all diffraction peaks of Mo-CQDs except peaks at 2θ = 29° and 34.4° could be indexed to carbon (JCPDS No. 46-943) and the diffraction peaks at 2θ = 29° and 34.4° correspond to (220) and (400) of β-Mo_2C (JCPDS No. 45-1013). As expected, there was no diffraction peak that can be indexed to MoS_2. Furthermore, Fig. 3c displays that the partial enlargement of the peak for Mo-CQDs at 2θ = 45.4° slightly shifted to smaller angles in comparison with carbon. This situation may result from Mo doping into CQDs. Therefore, the results of XPS, FTIR and XRD indicated that partial Mo and S were doped into CQDs, and partial Mo existed in the form of carbide, coupling with CQDs.

The photoluminescence and UV-vis absorption spectra of Mo-CQDs are shown in Fig. S2 (ESI†), and they exhibited an emission-dependent wavelength. The quantum yield of Mo-CQDs at 320 nm excitation was determined to be 3.65% using an Edinburgh FLS920 phosphorimeter. The aqueous solution of Mo-CQDs was blue under UV excitation at 365 nm and colorless under daylight. In contrast, a sample was prepared under the same conditions and using the same process but without the addition of MoS_2 powder. The product was almost colorless under UV light of 365 nm with a very low yield. The yield of Mo-CQDs was 35 times higher than that of pure CQDs (Table S1, ESI†). All the above tests indicated that the introduction of Mo and S atoms could crosslink the carbon based materials and obviously facilitated the formation of CQDs, as well as significantly enhancing the yield of CQDs.

3.2 Study of peroxidase-like catalytic activity of Mo-CQDs

The peroxidase mimetic catalytic activity of Mo-CQDs was investigated through catalytic oxidation of the TMB–H_2O_2 reaction. The UV-vis spectra and photographs of Mo-CQDs/TMB, H_2O_2/TMB, and Mo-CQDs/H_2O_2/TMB systems were recorded after they

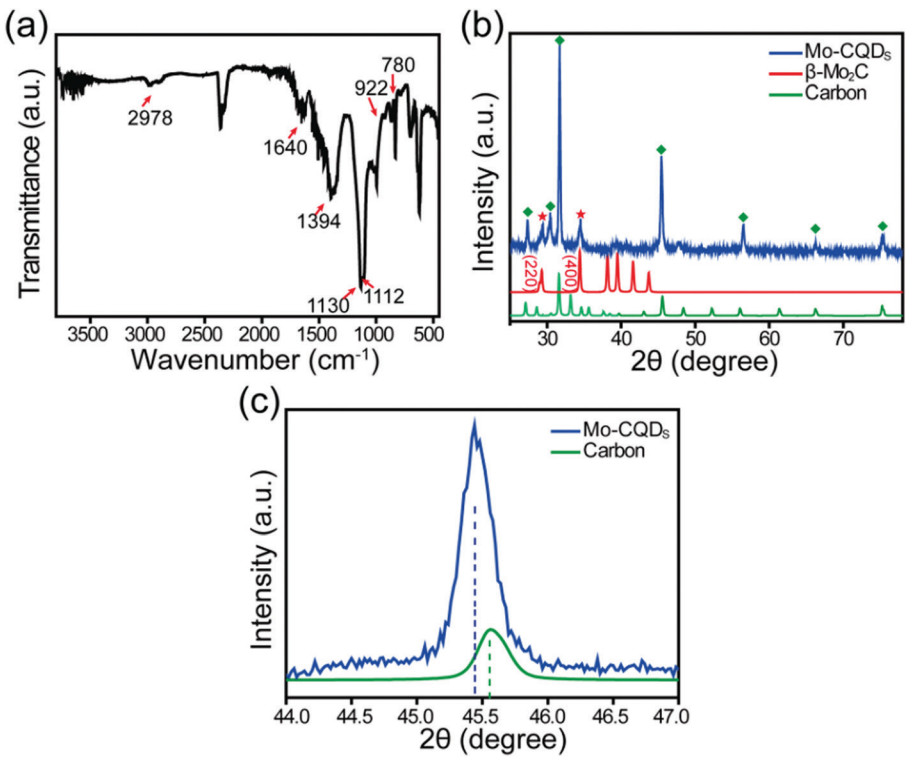

Fig. 3 (a) FTIR spectra and (b) XRD pattern of the Mo-CQDs. (c) Partial enlargement of XRD pattern of Mo-CQDs.

were mixed and incubated for 30 min, respectively. As shown in Fig. 4a, there was no absorbance in the Mo-CQDs/TMB system, demonstrating that no oxidation reaction of TMB occurred. A weak UV-vis absorbance and tinged blue color of solution were obtained in the H_2O_2/TMB system, suggesting that the reaction rate of TMB and H_2O_2 was low. However, the UV-vis absorbance of the Mo-CQDs/H_2O_2/TMB system was remarkably enhanced and displayed intense characteristic absorbance at 369 nm and 652 nm. In addition, the color of the solution became bright blue. This indicated that Mo-CQDs catalyzed the oxidation of TMB by H_2O_2. Fig. 4b displays the time dependent absorbance change of the above three reaction systems, confirming the high catalytic activity of Mo-CQDs. Moreover, Mo-CQD catalytic oxidation of the TMB–H_2O_2 reaction began to stabilize after 30 min of incubation.

The effects of pH and temperature on Mo-CQD catalytic capability were investigated. As shown in Fig. S3 (ESI†), the peroxidase mimetic activity of Mo-CQDs was also affected by pH and temperature, similar to natural peroxidase (HRP).[16] The catalytic activity of Mo-CQDs in acidic solutions was obviously better than that in alkaline solutions and pH 4.0 was optimum. Interestingly, the Mo-CQDs/H_2O_2/TMB system at room temperature had a similar catalytic activity as that at 30 °C, 35 °C and 40 °C. The high catalytic capacity at room temperature makes it easier for its application in a portable test kit.

The steady state kinetics of the Mo-CQDs/H_2O_2/TMB system was used to further investigate the peroxidase mimetic activity of Mo-CQDs by keeping the concentration of TMB or H_2O_2 constant. Fig. 5 depicts relations between velocity and the concentrations of TMB or H_2O_2. Results showed that typical Michaelis–Menten Curves were achieved for both TMB and H_2O_2. The steady state kinetics parameters, the maximum reaction velocity (V_{max}) and the Michaelies constant (K_m), were calculated by using the Lineweaver–Burk plot, $1/\upsilon = (K_m/V_{max}) \times (1/[s]) + 1/V_{max}$. The initial reaction rate (υ) at different concentrations of substrates was calculated by using the Beer–Lambert law equation. K_m approximately indicates the affinity of an enzyme to a substrate. When the value of K_m is smaller, the affinity of the enzyme to the substrate is stronger. Table S2 (ESI†) provides the K_m and V_{max} of different nanomaterials with various peroxidase mimics and HRP. The K_m value of Mo-CQDs in this work with H_2O_2 as a substrate was substantially lower in comparison with those of HRP, carbon nanodots, N-GQDs, GQDs, BNNS@CuS, AuNPs@MoS_2QDs and N-GQDs, clearly demonstrating that the Mo-CQDs possessed a stronger affinity toward H_2O_2 than those of the above listed substances. Furthermore, the K_m value of Mo-CQDs using TMB as a substrate was lower in comparison with that of HRP, silicon dots and N-GQDs. Meanwhile the V_{max} of Mo-CQDs with the same substrate was higher than those substances, indicating that Mo-CQDs in this work possessed a stronger affinity and higher catalytic activity for TMB than those substances. Recent research studies have demonstrated that the enhancement of affinity of nanozymes to substrates could boost the peroxidase-like activity of nanozymes.[56,57] In the current study, the high affinity between the Mo-CQDs and TMB or H_2O_2 could be one reason why Mo-CQDs possessed superior catalytic activity when either TMB or H_2O_2 acted as a substrate.

The catalytic mechanism of functionalized Mo-CQDs was thought to be that TMB could integrate with Mo-CQDs, and then lone-pair electrons in TMB amino groups transferred to the Mo-CQDs,[21,23] leading to an increase in the electron density and mobility of the Mo-CQDs, which resulted in the acceleration of electron transfer from Mo-CQDs to H_2O_2.[58,59] The investigation of chemical composition and surface groups of the Mo-CQDs demonstrated that the Mo-CQDs contained graphitic sp^2 carbon atoms and carboxylic/carbonyl moieties on their surfaces (Fig. 2 and 3). A density functionalized theory study showed that the graphene surfaces with functionalized carboxylic and carbonyl moieties played a crucial role in the reduction reaction of H_2O_2.[60] Previous research also demonstrated that carboxylic and carbonyl moieties of GQDs were the substrate-binding sites and catalytic active sites, respectively.[61] Therefore, in our case, we speculate that the carboxylic/carbonyl functionalized Mo-CQDs may have a similar function. Moreover, according to related literature, MoS_2 quantum dots and MoS_2 nanosheets could work as peroxidase mimetics, which would facilitate the electron transfer between TMB and H_2O_2.[19,40] Similarly, Mo, S doping in the CQDs may further accelerate the electron transfer between TMB and H_2O_2. Consequently, the oxidation rate of TMB–H_2O_2 reaction was accelerated.

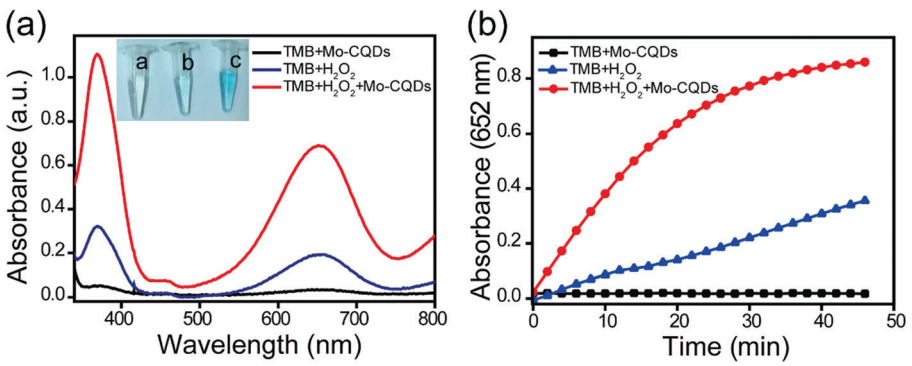

Fig. 4 (a) Absorbance spectra of different reaction systems: (b) time dependent absorbance change of different reaction systems. TMB + Mo-CQDs (black curve), TMB + H_2O_2 (red curves); TMB + H_2O_2 + Mo-CQDs (blue curves). The inset shows the visible color of different reaction systems: (a) TMB + Mo-CQDs, (b) TMB + H_2O_2, and (c) TMB + H_2O_2 + Mo-CQDs. The concentration of TMB was 1.0 mM and the concentration of H_2O_2 was 0.05 mM.

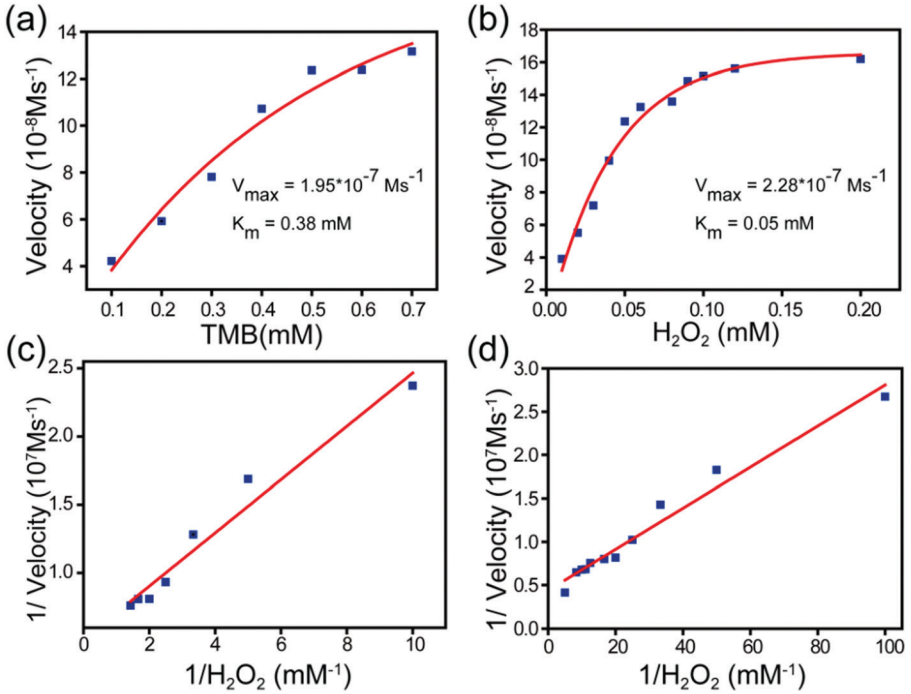

Fig. 5 Steady state kinetic assay of Mo-CQDs. Experiments were performed in 300 μL of 0.2 M sodium acetate buffer (pH 4.0) with 3.3 μg mL^{-1} Mo-CQDs at room temperature. (a) The concentration of H_2O_2 was 0.1 mM. (b) The concentration of TMB was 1 mM.

3.3 Detection of H_2O_2 and cholesterol using Mo-CQDs as a catalyst

The mechanism of colorimetric detection of H_2O_2 and cholesterol is illustrated in Fig. 6a. The oxidation of the TMB–H_2O_2 reaction could be catalyzed by Mo-CQDs to generate oxidized TMB (ox-TMB) with a maximum absorption at 652 nm. The concentration of H_2O_2 in a suitable range could be obtained by detecting UV-vis absorbance at 652 nm and estimated by the color of solution. In addition, combining with cholesterol oxidase (Chox)-triggered oxidation of cholesterol, the Mo-CQD-based cascade colorimetric biosensor could be applied in the detection of cholesterol. As depicted in Fig. 6b, the UV absorption was gradually enhanced with the increase in the concentration of H_2O_2 from 0 to 0.05 mM under optimal conditions. Simultaneously, the color of the solution gradually changed from colorless to dark blue as the concentration of H_2O_2 increased (inset of Fig. 6a). A good linear relationship (R^2 = 0.9955) in the range of 0.005–0.05 mM was obtained (Fig. 6c), demonstrating that the Mo-CQD catalytic system with a high sensitivity for H_2O_2 could be utilized in monitoring the enzyme-triggered reaction wherein H_2O_2 was one of the catalysis products. As a proof-of-concept, the UV absorption gradually increased with the increase in the concentrations of cholesterol under optimal conditions (Fig. 6d). In addition, the variety of solution color from colorless to blue was obvious as the concentration of cholesterol increased (inset in Fig. 6d). These results demonstrated that the proposed strategy could be applied in detecting cholesterol by visual observation even at low concentrations (0.05 mM). A linear relationship in the range of 0.01 to 0.6 mM was obtained with the detection limit for cholesterol of 7 μM (LOD = 3S/N) (Fig. 6e). The linear regression equation is $y = 1.38x + 0.02$ (R^2 = 0.9905), where y is the UV-vis absorbance intensity at 652 nm, and x is the concentration of cholesterol. Comparison of analytical performance of cholesterol biosensors is displayed in Table 1. The established sensor exhibited a superior or competitive analytic performance in comparison with other homogeneous cholesterol biosensors. Further, the preparation of the Mo-CQDs possessed some advantages, such as simplification, convenience and low cost, compared with those nanomaterials listed in Table 1, indicating that the Chox/Mo-CQDs platform was more suitable for the detection of cholesterol.

The selectivity of the cholesterol biosensor was evaluated by investigating the response of the sensing platform toward co-existing interferences (glucose, urea, uric acid, ascorbic acid and cysteine) under the same experimental conditions. As shown in Fig. 7a, the absorbance intensity of the system toward the above interference substances (2 mM) was very weak and was close to that of the control group, significantly lower than that of 0.4 mM cholesterol. This result demonstrated that the biosensor platform possessed excellent specificity for recognizing cholesterol.

The stability of the sensing platform is another crucial factor for practical application. The stability of the Mo-CQD-based biosensor was investigated by detecting the same cholesterol concentration (0.5 mM) intermittently (every 5 days) during a 20 day period. As shown in Fig. 7b, no apparent changes in the absorption intensity at 652 nm were observed during its storage for 20 days, suggesting that the constructed cholesterol biosensor had a good stability, which was mainly attributed to excellent stability of the Mo-CQDs.

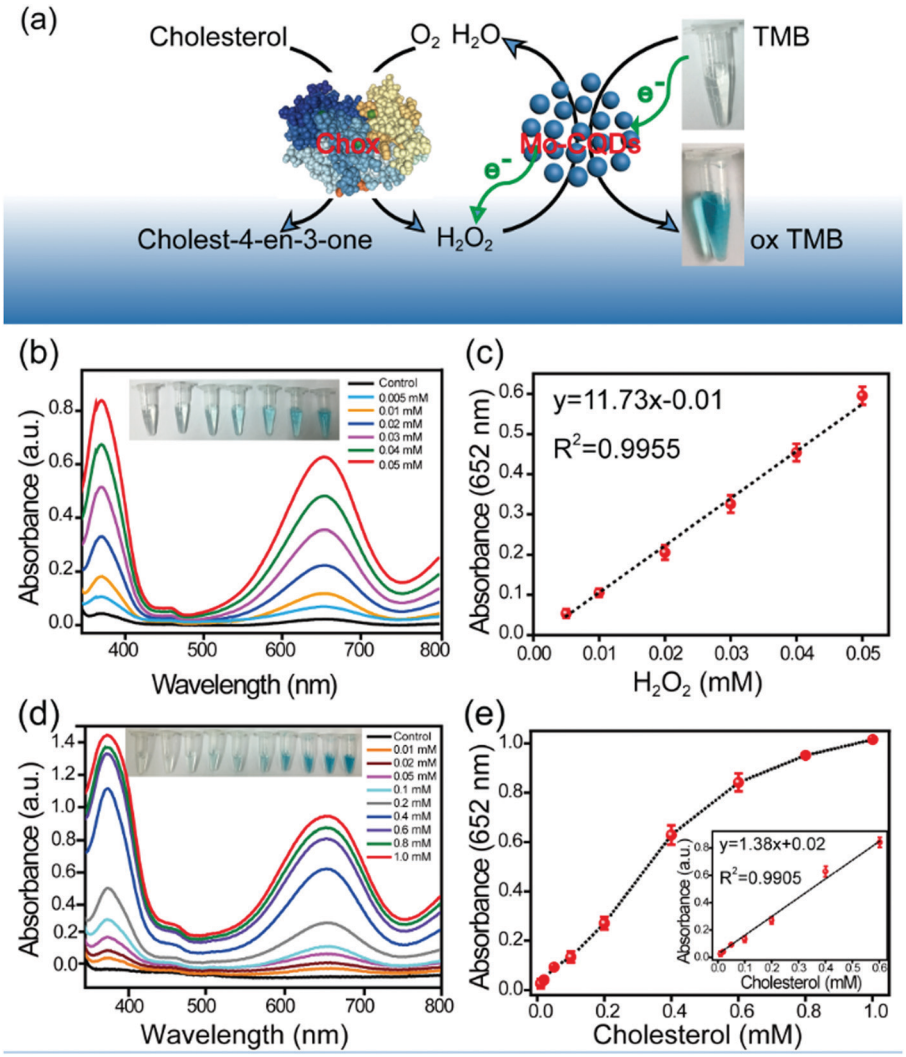

Fig. 6 (a) Schematic illustration of the colorimetric detection of cholesterol using cholesterol oxidase (Chox) and Mo-CQDs. (b and d) UV-vis spectra of colorimetric detection of H_2O_2 and cholesterol based on Mo-CQDs. The inset of (b and d) presents the corresponding images of visible color in the presence of H_2O_2. (c, inset of (e)) Linear calibration curves for H_2O_2 and cholesterol detection. (e) Calibration curves for cholesterol.

Table 1 Comparison of analytical performances of cholesterol biosensors based on various nanomaterials

Sensing materials	Detection method	Linear range (μM)	Detection limit (μM)	Ref.
Chox/Fe_2O_3	Amperometry	100–8000	18	62
AgNPs/GCE	Amperometry	100–20 000	25.8	63
BNNS@CuS	Colorimetry	10–100	2.9	64
GQD	Colorimetry	20–600	6	33
Au/MoS_2	Colorimetry	40–1000	15	18
Mo-CQDs	Colorimetry	10–600	7	Present work

3.4 Analysis of serum samples employing the proposed biosensor

To estimate the possibility of the proposed biosensor for cholesterol detection in clinical samples, the fabricated colorimetric approach was applied in detecting total cholesterol in serum samples. The total cholesterol in serum was composed of free cholesterol and cholesterol ester that could be converted to free cholesterol by cholesterol esterase. Therefore, the total cholesterol could be detected by adding both cholesterol esterase and Chox. In the testing process, 2.0 μL of serum sample was added into 50 μL and 48 μL of phosphate buffer containing cholesterol esterase for incubating for 30 min. Then, sodium acetate buffer containing Mo-CQDs and TMB was introduced into the mixture. Finally, the total cholesterol in serum was detected by UV-vis spectral measurements. Fig. 8 shows the response of the proposed biosensor toward three volunteers' serum samples. These results can be directly evaluated by the naked eye, indicating the potential to develop a cholesterol portable test kit. Table 2 reveals the detection results of total cholesterol in three volunteers' serum. The relative deviation was less than 10% compared with those of the clinical detection, which agreed well with those provided by the hospital. The relative deviation was calculated by the equation of relative deviation = $(F - F_0)/F_0 \times 100\%$, where F_0 stands for the value determined by the hospital method, and F stands for the value determined by

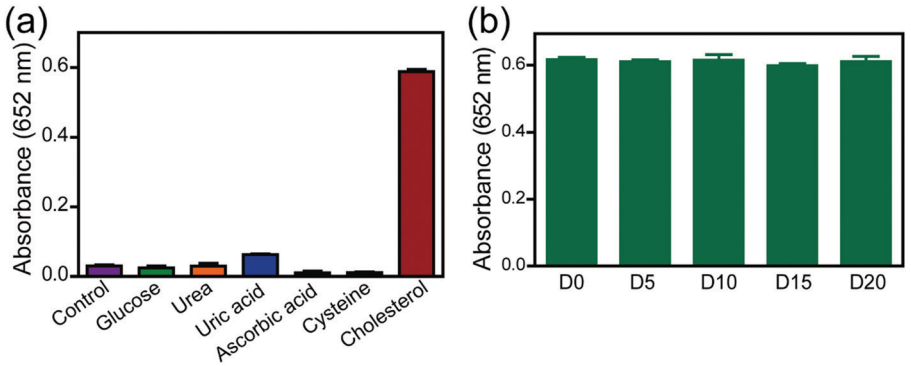

Fig. 7 (a) Selectivity of the sensing platform based on the Mo-CQDs with glucose, urea, uric acid, ascorbic acid and cysteine as control groups. The concentration of cholesterol was 0.4 mM. The concentration of others was 2 mM. (b) The stability of the cholesterol biosensor based on the Mo-CQDs. All error bars were estimated from three replicate measurements.

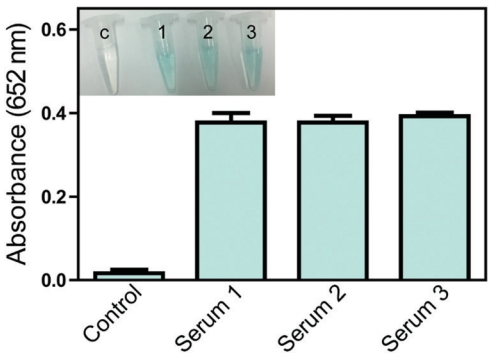

Fig. 8 Determination of total cholesterol in human serum samples. Inset: The images of the corresponding samples.

Table 2 Total cholesterol determination in human serum samples

Samples	Determined in the hospital (mM)	Determined by the proposed method (mM)	Relative deviation (%)
Serum 1	7.85	7.83 ± 0.69	−0.25
Serum 2	8.37	7.68 ± 0.28	−8.24
Serum 3	7.75	8.45 ± 0.31	9.03

the proposed approach. Most hospitals employ cholesterol determination kits to detect the total cholesterol at present. The kits mainly consist of natural peroxidase (HRP), HRP substrate, cholesterol esterase and cholesterol oxidase. Compared with the commercial method, the proposed approach replaced HRP with the Mo-CQDs that possessed the merits of low cost, high stability and facile preparation. The above results demonstrated the promising application of the proposed approach in clinical diagnosis.

4 Conclusion

In summary, we have successfully prepared Mo, S co-doped CQDs with characteristics of robust peroxidase-like activity, being cost effective, easy synthesis, good dispersion and good biocompatibility, which were synthesized by one-step solvothermal treatment of ethanol with the assistance of MoS_2. The doping of Mo, S in the CQDs significantly facilitated the formation of CQDs and may further enhance the peroxidase-like activity of CQDs. The Mo-CQDs could catalyze the TMB–H_2O_2 reaction to generate colored ox-TMB, which possessed high affinity toward both TMB and H_2O_2. The cascade colorimetric biosensor based on the Mo-CQDs and cholesterol oxidase for cholesterol detection was established, exhibiting high sensitivity, excellent selectivity and good stability. In addition, the level of cholesterol could be easily evaluated by observation of solution color with the naked eye. Furthermore, total cholesterol in human serum could be measured by the proposed approach, which was well in agreement with that of clinical detection. The fabricated sensing platform exhibits promising potential in clinical diagnosis and portable test kits.

Conflicts of interest

There are no conflicts of interest to declare.

Acknowledgements

This work was supported by grants from the China Postdoctoral Science Foundation (No. 2018M640282), the National Nature Science Foundation of China (61304242 and 61520106003) and the Program for Chang Jiang Scholars and Innovative Research Team in University (IRT_17R47).

Notes and references

1 E. Priyadarshini and K. Rawat, *J. Mater. Chem. B*, 2017, **5**, 5425–5432.
2 F. R. Maxfield and I. Tabas, *Nature*, 2005, **438**, 612–621.
3 S. Soylemez, S. O. Hacioglu, M. Kesik, H. Unay, A. Cirpan and L. Toppare, *ACS Appl. Mater. Interfaces*, 2014, **6**, 18290.
4 L. Sarah, W. Gary, C. Robert, S. Paul, E. Jonathan, H. Jim, Q. Nawab, P. Richard and C. Rory, *Lancet*, 2007, **370**, 1829–1839.
5 K. Wang, H. Ren, N. Li, X. Tan and F. Dang, *Talanta*, 2018, **188**, 708–713.

6 M. Duan, Y. Peng, L. Zhang, X. Wang, J. Ge, J. Jiang and R. Yu, *Anal. Methods*, 2013, **5**, 2182–2187.
7 N. Agnihotri, A. D. Chowdhury and A. De, *Biosens. Bioelectron.*, 2015, **63**, 212–217.
8 S. Xu, Y. Wang, D. Zhou, M. Kuang, D. Fang, W. Yang, S. Wei and L. Ma, *Sci. Rep.*, 2016, **6**, 39157.
9 J. Du, L. Jiang, Q. Shao, X. Liu, R. S. Marks, J. Ma and X. Chen, *Small*, 2013, **9**, 1467–1481.
10 W. Hui and W. Erkang, *Chem. Soc. Rev.*, 2013, **42**, 6060–6093.
11 Y. Ding, H. Liu, L.-N. Gao, M. Fu, X. Luo, X. Zhang, Q. Liu and R.-C. Zeng, *J. Alloys Compd.*, 2019, **785**, 1189–1197.
12 C. Jin, J. Lian, Y. Gao, K. Guo, K. Wu, L. Gao, X. Zhang, X. Zhang and Q. Liu, *ACS Sustainable Chem. Eng.*, 2019, **7**, 13989–13998.
13 Q. Liu, Y. Yang, X. Lv, Y. Ding, Y. Zhang, J. Jing and C. Xu, *Sens. Actuators, B*, 2017, **240**, 726–734.
14 H. Liu, Y.-N. Ding, B. Yang, Z. Liu, X. Zhang and Q. Liu, *ACS Sustainable Chem. Eng.*, 2018, **6**, 14383–14393.
15 L. Gao, K. M. Giglio, J. L. Nelson, H. Sondermann and A. J. Travis, *Nanoscale*, 2014, **6**, 2588–2593.
16 L. Gao, J. Zhuang, L. Nie, J. Zhang, Y. Zhang, N. Gu, T. Wang, J. Feng, D. Yang and S. Perrett, *Nat. Nanotechnol.*, 2007, **2**, 577–583.
17 A. Li, X. Mu, T. Li, H. Wen, W. Li, Y. Li and B. Wang, *Nanoscale*, 2018, **10**, 11948–11954.
18 N. R. Nirala, S. Pandey, A. Bansal, V. K. Singh, B. Mukherjee, P. S. Saxena and A. Srivastava, *Biosens. Bioelectron.*, 2015, **74**, 207–213.
19 Vinita, N. R. Nirala and R. Prakash, *Sens. Actuators, B*, 2018, **263**, 109–119.
20 A. X. Zheng, Z. X. Cong, J. R. Wang, J. Li, H. H. Yang and G. N. Chen, *Biosens. Bioelectron.*, 2013, **49**, 519–524.
21 S. Yujun, Q. Konggang, Z. Chao, R. Jinsong and Q. Xiaogang, *Adv. Mater.*, 2010, **22**, 2206–2210.
22 M. Chen, B. Yang, J. Zhu, H. Liu, X. Zhang, X. Zheng and Q. Liu, *Mater. Sci. Eng., C*, 2018, **90**, 610–620.
23 Y. Song, X. Wang, C. Zhao, K. Qu, J. R. Dr and X. Q. Prof, *Chem. – Eur. J.*, 2010, **16**, 3617–3621.
24 C. Qiong, L. Meiling, Z. Jiangna, P. Xue, C. Xiaojiao, M. Naxiu, Y. Bangda, L. Haitao, Z. Youyu and Y. Shouzhuo, *Chem. Commun.*, 2014, **50**, 6771–6774.
25 J. Lian, P. Liu, C. Jin, Z. Shi, X. Luo and Q. Liu, *Microchim. Acta*, 2019, **186**, 332.
26 J. Hassanzadeh, A. Khataee and H. Eskandari, *Sens. Actuators, B*, 2018, **259**, 402–410.
27 D. Ma, J. Yu, W. Yin, X. Zhang, L. Mei, Y. Zu, L. An and Z. Gu, *Chem. – Eur. J.*, 2018, **24**, 15868–15878.
28 Y. Wu, Y. Ma, G. Xu, F. Wei, Y. Ma, Q. Song, X. Wang, T. Tang, Y. Song, M. Shi, X. Xu and Q. Hu, *Sens. Actuators, B*, 2017, **249**, 195–202.
29 D. C. Green, M. A. Holden, M. A. Levenstein, S. Zhang, B. R. G. Johnson, J. Gala de Pablo, A. Ward, S. W. Botchway and F. C. Meldrum, *Nat. Commun.*, 2019, **10**, 206.
30 Y. Zhang, K. F. Chan, B. Wang, P. W. Y. Chiu and L. Zhang, *Sens. Actuators, B*, 2018, **271**, 128–136.
31 T. H. Kim, J. P. Sirdaarta, Q. Zhang, E. Eftekhari, J. St. John, D. Kennedy, I. E. Cock and Q. Li, *Nano Res.*, 2018, **11**, 2204–2216.
32 N. R. Nirala, S. Abraham, V. Kumar, A. Bansal, A. Srivastava and P. S. Saxena, *Sens. Actuators, B*, 2015, **218**, 42–50.
33 L. Lin, X. Song, Y. Chen, M. Rong, T. Zhao, Y. Wang, Y. Jiang and X. Chen, *Anal. Chim. Acta*, 2015, **869**, 89–95.
34 L. Yan, H. Yue, Z. Yang, S. Gaoquan, D. Lier, H. Yanbing and Q. Liangti, *Adv. Mater.*, 2011, **23**, 776–780.
35 P. Xu, C. Wang, D. Sun, Y. Chen and K. Zhuo, *Chem. Res. Chin. Univ.*, 2015, **31**, 730–735.
36 Y. Dong, H. Pang, H. B. Yang, C. Guo, J. Shao, Y. Chi, C. M. Li and T. Yu, *Angew. Chem., Int. Ed.*, 2013, **52**, 7800–7804.
37 Y.-W. Bao, X.-W. Hua, H.-H. Ran, J. Zeng and F.-G. Wu, *J. Mater. Chem. B*, 2019, **7**, 296–304.
38 Y. Ma, Y. Cen, M. Sohail, G. Xu, F. Wei, M. Shi, X. Xu, Y. Song, Y. Ma and Q. Hu, *ACS Appl. Mater. Interfaces*, 2017, **9**, 33011–33019.
39 J. Lei, X. Lu, G. Nie, Z. Jiang and C. Wang, *Part. Part. Syst. Charact.*, 2015, **32**, 886–892.
40 T. Lin, L. Zhong, L. Guo, F. Fu and G. Chen, *Nanoscale*, 2014, **6**, 11856–11862.
41 W. Yin, L. Yan, J. Yu, G. Tian, L. Zhou, X. Zheng, X. Zhang, Y. Yong, J. Li, Z. Gu and Y. Zhao, *ACS Nano*, 2014, **8**, 6922–6933.
42 Q. Chang, X. Han, C. Xue, J. Yang and S. Hu, *Chem. Commun.*, 2017, **53**, 2343–2346.
43 H. Ding, J.-S. Wei, P. Zhang, Z.-Y. Zhou, Q.-Y. Gao and H.-M. Xiong, *Small*, 2018, **14**, 1800612.
44 X. Wang, Q. Wu, K. Jiang, C. Wang and C. Zhang, *Sens. Actuators, B*, 2017, **252**, 183–190.
45 S. Sahu, B. Behera, T. K. Maiti and S. Mohapatra, *Chem. Commun.*, 2012, **48**, 8835–8837.
46 B. Lei, Z. Zhi-Ling, T. Zhi-Quan, Z. Li, L. Cui, L. Yi, Q. Baoping and P. Dai-Wen, *Adv. Mater.*, 2011, **23**, 5801–5806.
47 X. Miao, X. Yan, D. Qu, D. Li, F. F. Tao and Z. Sun, *ACS Appl. Mater. Interfaces*, 2017, **9**, 18549–18556.
48 D. Qu, M. Zheng, P. Du, Y. Zhou, L. Zhang, D. Li, H. Tan, Z. Zhao, Z. Xie and Z. Sun, *Nanoscale*, 2013, **5**, 12272–12277.
49 S. Li, Y. Li, J. Cao, J. Zhu, L. Fan and X. Li, *Anal. Chem.*, 2014, **86**, 10201–10207.
50 M. Sevilla and A. B. Fuertes, *Microporous Mesoporous Mater.*, 2012, **158**, 318–323.
51 Z. Yang, Z. Yao, G. Li, G. Fang, H. Nie, Z. Liu, X. Zhou, X. a. Chen and S. Huang, *ACS Nano*, 2012, **6**, 205–211.
52 X. Liu, Y. Hao, J. Shu, H. M. K. Sari, L. Lin, H. Kou, J. Li, W. Liu, B. Yan, D. Li, J. Zhang and X. Li, *Nano Energy*, 2019, **57**, 414–423.
53 H. Wang, Y. Cao, C. Sun, G. Zou, J. Huang, X. Kuai, J. Zhao and L. Gao, *ChemSusChem*, 2017, **10**, 3540–3546.
54 S. Chen, S. Yupeng, W. Jing and L. Yun, *Nanoscale*, 2014, **6**, 9139–9147.
55 Y. Hu, J. Yang, L. Jia and J. S. Yu, *Carbon*, 2015, **93**, 999–1007.
56 B. Liu and J. Liu, *Nanoscale*, 2015, **7**, 13831–13835.
57 Y.-M. Wang, J.-W. Liu, G. B. Adkins, W. Shen, M. P. Trinh, L.-Y. Duan, J.-H. Jiang and W. Zhong, *Anal. Chem.*, 2017, **89**, 12327–12333.

58 K. Jong-Ho, D. A. Heller, J. Hong, P. W. Barone, S. Changsik, Z. Jingqing, L. J. Trudel, G. N. Wogan, S. R. Tannenbaum and M. S. Strano, *Nat. Chem.*, 2009, **1**, 473–481.
59 S. Wenbing, W. Qinlong, L. Yijuan, C. Zhiliang, C. Shihong, Z. Huzhi and H. Yuming, *Chem. Commun.*, 2011, **47**, 6695–6697.
60 G. L. Luque, M. I. Rojas, G. A. Rivas and E. P. M. Leiva, *Electrochim. Acta*, 2011, **56**, 523–530.
61 H. Sun, A. Zhao, N. Gao, K. Li, J. Ren and X. Qu, *Angew. Chem., Int. Ed.*, 2015, **54**, 7176–7180.
62 A. Umar, R. Ahmad, S. W. Hwang, S. H. Kim, A. Al-Hajry and Y. B. Hahn, *Electrochim. Acta*, 2014, **135**, 396–403.
63 S. Nantaphol, O. Chailapakul and W. Siangproh, *Sens. Actuators, B*, 2015, **207**, 193–198.
64 Y. Zhang, Y. N. Wang, X. T. Sun, L. Chen and Z. R. Xu, *Sens. Actuators, B*, 2017, **246**, 118–126.